Pyrolysis of Biomass Impregnated With Ammonium Dihydrogen Phosphate for Polygeneration of Phenol and Supercapacitor Electrode Material

Kai Li, Bo Wang, Dana Bolatibieke, Dong-hong Nan and Qiang Lu*

National Engineering Laboratory for Biomass Power Generation Equipment, North China Electric Power University, Beijing, China

A new method was proposed for polygeneration of phenol and supercapacitor electrode material from pyrolysis of biomass impregnated with ammonium dihydrogen phosphate ($NH_4H_2PO_4$). The pyrolysis experiments were executed to demonstrate the product distributions under different $NH_4H_2PO_4$-to-poplar (PA-to-PL) ratios and pyrolysis temperatures in a lab-scale device. The results revealed that the phenol yield attained its optimal value of 4.57 wt% with a satisfactory selectivity of 20.09% at 500°C under PA-to-PL ratio of 0.6. The pyrolytic solid product obtained at this condition was then subjected to high temperature activation directly without additional activators to prepare N and P co-doped activated carbon (NPAC) as supercapacitor. The physicochemical analysis of NPAC showed that the N and P contents in NPAC reached 3.75 and 3.65 wt%, respectively. The electrochemical experiments executed in a three-electrode system indicated that the NPAC exhibited promising electrochemical performance with a satisfactory capacitance of 181.3 F g^{-1} at 1 A g^{-1}.

Keywords: biomass, $NH_4H_2PO_4$, pyrolysis, phenol, supercapacitor

INTRODUCTION

Lignocellulosic biomass can be quickly converted into liquid, gaseous and solid products by fast pyrolysis technology (Lu et al., 2018b; Wang et al., 2018a). The efficient utilization of the pyrolytic products directly determines the application of this technology. Among the three biomass pyrolytic products, the liquid product (bio-oil) is usually the dominant product with potential applications as liquid fuels or raw chemical materials (Kan et al., 2016; Chen et al., 2019). Particularly, there are various value-added chemicals in bio-oil, which allows their separation and purification to obtain specific compounds (Brueckner et al., 2020). However, the contents of most chemicals in bio-oil are extremely low, making the conventional bio-oil fairly difficult to be utilized (Chen et al., 2014; Muneer et al., 2019). Therefore, tireless and unremitting endeavors have been devoted to regulating the biomass pyrolysis process pertinently for preparing specific bio-oils abundant in target valuable products, such as levoglucosenone (Ye et al., 2017), furfural (Su et al., 2020), phenol (Chang et al., 2018), and so on.

Phenol is one of high value-added compounds derived from biomass pyrolysis, widely used in synthetic fibers, medicine, pesticides, and so on. It is mainly decomposed from lignin (Lazaridis et al., 2018). Because of the irregular lignin structures, fast pyrolysis of lignin or biomass will inevitably form hundreds of phenolic compounds in bio-oil, rather than any specific phenolics (Dong et al., 2012; Duan et al., 2019). Hitherto, various researches have been concentrated on the selective pyrolysis of biomass to produce mixed or specific phenolic compounds (Yaman et al., 2018). Lu et al. (2013) employed K_3PO_4 for the biomass pyrolysis to prepare phenolics. The maximum phenolics content of 64.2% (in GC peak area%) was obtained at 500°C with the K_3PO_4 content of 50.51 wt%. Among the phenolics, phenol was a major product with a high peak area% of 14.3%. Bu et al. (2012) conducted the biomass pyrolysis experiments catalyzed by acid-washed activated carbon (AC). Mixed phenolics with the concentration of 66.9% (in peak area%) were obtained, accompanied with the phenol concentration of 38.9%.

Although mixed phenolics could be selectively prepared from biomass catalytic pyrolysis and phenol was the main compound in the mixed phenolics, the variety of phenolics mixture in the liquid product would inhibit the further purification of phenol. Therefore, it is fatal to further promote the yield and selectivity of phenol. Currently, only limited researches have been performed on the selective preparation of phenol. Our group put forward a creative method to obtain phenol from catalytic decomposition of biomass by impregnation of K_3PO_4 or blended with magnetic K_3PO_4/Fe_3O_4 solid catalyst under hydrogen atmosphere (Lu et al., 2018c; Zhang et al., 2019). The phenol yields reached 5.3 and 4.3 wt%, respectively, both with excellent selectivity of ~18%. The hydrogen source in the pyrolysis process facilitated the elimination of substitutes of phenolic compounds to generate phenol (Liu et al., 2014; Zhang et al., 2019). Differed from conventional techniques to produce phenol from lignin, Zhang et al. (2018a) established a new and unique system to selectively produce phenol from non-lignin materials, such as cellulose. With the assistant of AC prepared by H_3PO_4 activation, the phenol from cellulose pyrolysis achieved an excellent selectivity of 99.02% (in peak area%) under 450°C. Wherein, the P-containing groups in the AC were supposed to be responsible for the generation of phenol.

In addition to the liquid product, solid product (char) is usually an important by-product of biomass fast pyrolysis process. Char is widely used as solid fuels or further processed to ACs (Xu et al., 2020), carbon-based fertilizers (Liang et al., 2016), supercapacitor electrode materials (Lu et al., 2018a), and so on. The utilization of char to prepare supercapacitor electrode materials has been drawing increasing attention due to the availability, low cost and renewability of raw materials (Wang and Wang, 2019; Kim et al., 2020). However, raw char product obtained directly from lignocellulosic biomass pyrolysis process exhibited unsatisfactory capacitive performance because of the limited surface area and active sites (Zhao et al., 2017). Therefore, activation and incorporation of heteroatoms (N, P, S, etc.) were adopted to improve porosity and functional groups of char materials (Wang et al., 2018b). Chen et al. (2016) synthesized the N doped carbon materials by subjecting

biomass successively to pyrolysis in the NH_3 atmosphere and KOH activation. The obtained AC possessed high nitrogen and specific surface area (SSA) with the specific capacitance (C_g) of 187 F g^{-1} at 1 A g^{-1}. Wang et al. (2013a,b) synthetized two N and P co-doped activated carbons (NPACs) for supercapacitors by carbonization of polyaniline impregnated with H_3PO_4 and glucose with $(NH_4)_3PO_4$. The corresponding C_gs of the NPACs at 0.05 A g^{-1} could reach 154.4 and 183.8 F g^{-1}, respectively. All of these studies suggested that incorporating N and P into carbon materials would be conducive to optimizing the electrochemical performance of carbon electrodes.

In present work, a new way was developed for the co-production of phenol and supercapacitor electrode material from pyrolysis of biomass impregnated with $NH_4H_2PO_4$. $NH_4H_2PO_4$ is an inexpensive and common chemical reagent with high N and P contents. The introduction of $NH_4H_2PO_4$ could alter the biomass pyrolysis process and also incorporate N and P in solid products. Therefore, polygeneration of phenol and supercapacitor electrode material could be achieved by the pyrolysis of $NH_4H_2PO_4$-impregnated biomass. A lab-scale device was employed for the pyrolysis experiments. The influences of $NH_4H_2PO_4$ to poplar (PA-to-PL) ratio and reaction temperature on the regulation of pyrolytic products were researched comprehensively. The optimal pyrolytic conditions for maximizing the phenol yield were identified. The solid products were then subjected to activation directly without additional activators to prepare NPACs.

MATERIALS AND METHODS

Materials

Poplar without bark was sampled from Hebei province in China. The received poplar was crushed firstly and then sieved into 0.1–0.15 mm particles. The dried particles were subjected to ultimate and proximate analyses referring to the methods in the previous literature (Li et al., 2017). The concentrations of carbon, hydrogen, sulfur as well as nitrogen on dry basis were directly measured to be 49.60, 6.31, 0.10, and 0.07 wt%, respectively, while the content of oxygen (43.67 wt%) was calculated by difference. Moreover, the contents of ash (0.25 wt%), volatile (86.44 wt%), and fixed carbon (13.31 wt%) were also quantified.

$NH_4H_2PO_4$ in analytical reagent grade was purchased from Macklin. Phenol in chromatography grade and KOH (AR, 90%) were purchased from Aladdin. Acetylene black, polytetrafluoroethylene (PTEF) and nickel foam were provided by Shanghai Saibo Chemical Co., Ltd.

The biomass samples impregnated with $NH_4H_2PO_4$ (PBs) were prepared via the incipient wetness impregnation method. For each PB sample, the quantity of poplar and the volume of $NH_4H_2PO_4$ aqueous solution were constant, while the concentrations of $NH_4H_2PO_4$ in the solutions were different to ensure the mass PA-to-PL ratios of 0.2, 0.6, 1.0, 1.4, and 1.8, respectively. The mixtures were subjected successively to ultrasonic oscillation for 40 min and oven-drying at 105°C. The samples were collected in desiccators for further use. The as-obtained PBs were donated as PB0.2, PB0.6, PB1.0, PB 1.4, and PB1.8, respectively.

Pyrolysis Experiments

Poplar and all the PBs were pyrolyzed in a lab-scale device as illustrated in **Figure 1**. In brief, the device was mainly integrated with a nitrogen gas cylinder, a tubular resistance furnace, a quartz tube pyrolysis reactor, and a condenser. In each experiment, N_2 was employed to remove air in the reactor and maintain the oxygen-free atmosphere for pyrolysis. Once the temperature of the reactor stabilized at the desired value (450, 500, 550, 600, and 650°C), the sample with a constant usage of 0.6 g was fed into the reactor continuously and uniformly in 5 min, and pyrolyzed for another 10 min.

The pyrolytic liquid and solid yields could be determined by weighing, while the gas yield was obtained by difference (Li et al., 2020). The solid product was collected from the reactor directly. Anhydrous alcohol was used to wash and dilute the liquid products. The water content was quantified using a Karl-Fisher moisture analyzer. The organic compounds were determined using a gas chromatograph instrument with their standard samples. The phenol yield was quantified by the external standard method.

Preparation of NPAC

The solid product obtained from pyrolysis of PB0.6 at 500°C was used to prepare NPAC according to the following method. A certain amount of the solid product was firstly transferred into a tubular resistance furnace (STGX-110-12, Henan Sante Furnace Technology Co., Ltd, China). Subsequently, the solid was heated to 800°C at 5°C min^{-1}, then hold for 1.5 h in nitrogen atmosphere. Following the high temperature activation, hot distilled water about 80°C was employed to wash the sample

repeatedly until a neutral pH was achieved. After being subjected to drying at 110°C, the final product was obtained and donated as NPAC. In addition, the pyrolytic solid product from pyrolysis of pure poplar at 500°C was also treated with the same method, the obtained solid was used as the control group and donated as PC.

Characterization of NPAC

An X-ray diffractometer (XRD, D8 advance) with Cu Kα radiation (λ = 0.15406 nm) was adopted to demonstrate the crystallographic structures of NPAC and PC. The data were recorded over the 2θ range of 10–90° with a scan rate of 6°/min. Chemical states of main elements (especially the N and P) on the NPAC surface were characterized by an X-ray photoelectron spectrometer (XPS, Thermo Escalab 250Xi) with Mg Kα radiation (1486.6 eV). All the binding energies were determined by referencing to the C1s peak at 284.8 eV. Porous characteristics were determined by nitrogen physisorption (ASAP2460) at 77 K. The SSA was calculated by the Barrett-Emmett-Teller (BET) method, while the pore volume and average pore diameter were determined by the Barrett-Joyner-Halenda (BJH) method. An inductively coupled plasma optical emission spectrometry (ICP-OES, Agilent ICPOES730) was adopted to measure the P content.

Electrochemical Tests of NPAC

The electrochemical tests of NPAC and PC were conducted using a three-electrode instrument (CH Instruments 760) with 6 M KOH solution. Wherein, the platinum plate was adopted as a counter electrode, and saturated calomel as a reference electrode. The working electrode was synthetized via mixing NPAC (or PC), acetylene black and PTEF completely to homogeneous slurry at
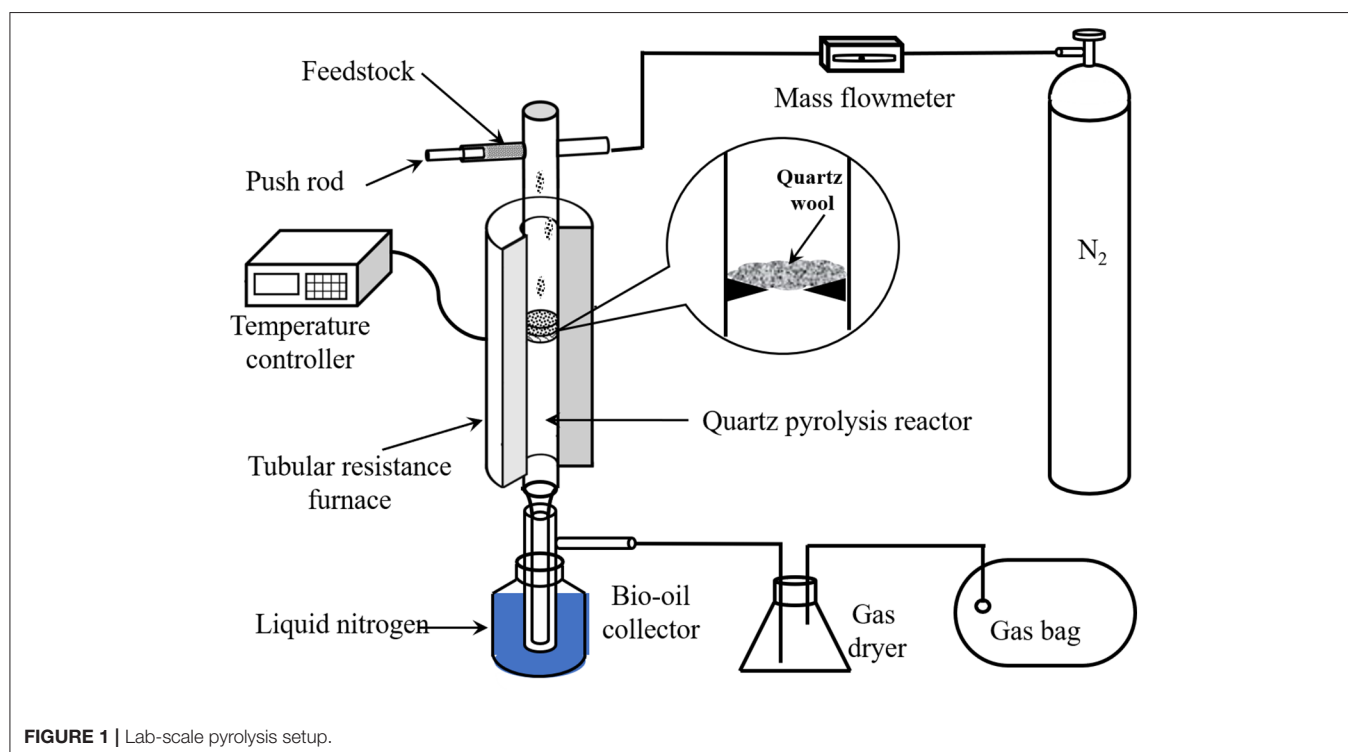

FIGURE 1 | Lab-scale pyrolysis setup.

the mass ratio of 8:1:1, which was subsequently daubed on a nickel foam (1×1 cm) uniformly, subjected to drying at 105°C, and pressed at 10 MPa.

The cyclic voltammetry (CV) tests were executed at various scan rates of 5, 10, 20, 40, and 100 mV s^{-1}. The galvanostatic charge/discharge (GCD) experiments were executed at current densities of 1, 2, 5, 10, and 20 A g^{-1}. The electrochemical impedance spectroscopy (EIS) properties were tested from 10 mHz to 100 kHz in 5 mV.

RESULTS AND DISCUSSION

Pyrolysis of Poplar Impregnated With NH$_4$H$_2$PO$_4$

Influence of PA-to-PL Ratio on the Pyrolysis of Poplar Impregnated With NH$_4$H$_2$PO$_4$

Poplar and PBs samples were employed for pyrolysis experiments at 500°C to elucidate the influences of PA-to-PL ratio on the distribution of main pyrolytic products (**Table 1**). For the pure poplar, the pyrolytic liquid yield was 50.75 wt%, accompanied with the gas and solid yields of 17.03 and 32.22 wt%, respectively. Whereas, the pyrolytic products yields changed greatly after the impregnation of NH$_4$H$_2$PO$_4$ on the poplar. For the pyrolysis of PB0.2, the yields of liquid, gas, and solid became 36.62, 14.45, and 48.93 wt%, resulting from the combined and interacted decomposition of poplar and NH$_4$H$_2$PO$_4$. It is notable that NH$_4$H$_2$PO$_4$ could decompose in the pyrolytic condition to concurrently produce large quantities of water and solid products. For pure NH$_4$H$_2$PO$_4$, its decomposition would generate around 61.74 wt% P$_2$O$_5$, 23.48 wt% water, and 14.78 wt% NH$_3$ at the pyrolytic temperature over 210°C (Di Blasi et al., 2007), higher than the yields of solid product and water from pure poplar. Whereas, in PB pyrolysis, the NH$_4$H$_2$PO$_4$ would not decompose singly (Li et al., 2016). Instead, it reacted with poplar decomposition products. The NH$_3$ derived from NH$_4$H$_2$PO$_4$ could react with O-containing functional groups to form N-containing compounds in the liquid product and achieve the incorporation of N in the solid product. **Figure S1** shows the typical ion chromatogram of the liquid product from pyrolysis of PB0.6 at 500°C. Apparently, phenol was the dominant product. The other organic compounds were all in low contents, which were mainly N-containing heterocyclic compounds (NHCs) and furfural. The NHCs mainly included pyridine, 2-methylpyridine and 3-pyridinol, they were believed to be derived from the Maillard reaction and further condensation reactions (Li et al., 2016; Chen et al., 2018a). Moreover, the parent acid from NH$_4$H$_2$PO$_4$ decomposition would act as the catalyst to deteriorate the dehydration and carbonization reactions in the pyrolysis process (Di Blasi et al., 2008). Considering the decomposition of NH$_4$H$_2$PO$_4$, the yield results still indicated that the impregnation of NH$_4$H$_2$PO$_4$ inhibited the pyrolytic devolatilization of poplar to generate liquid and gas products, while promoted the charring to obtain solid product. With the continuous increase of PA-to-PL ratio, the yields of all the products kept such trends. As a result, at PA-to-PL ratio of 1.8, the solid yield significantly rose to 67.59 wt%, accompanied with liquid and gas yields as low as 26.19 and 6.22 wt%, respectively. Moreover, the water content of liquid product increased monotonically from 34.30 wt% with pure poplar to 76.06 wt% at PA-to-PL ratio of 1.8. The increase of water content and decrease of liquid yield further confirmed the catalytic effects of NH$_4$H$_2$PO$_4$ to enhance dehydration and charring reactions, while inhibit the generation of organic compounds (Di Blasi et al., 2008).

As shown in **Table 1**, only a little phenol was generated from pyrolysis of pure poplar with an unsatisfactory yield of 0.49 wt% and a selectivity of 1.47%, which was entirely in accordance with the previous research (Zhang et al., 2019). With the impregnation of NH$_4$H$_2$PO$_4$, the phenol yield as well as the corresponding selectivity was increased dramatically. The phenol yield reached 3.07 wt% even at PA-to-PL ratio of 0.2. With the further rising of PA-to-PL ratio, the phenol yield exhibited a tendency of increasing first and then decreasing. At PA-to-PL ratio of 0.6, the phenol yield achieved its optimal value of 4.57 wt% with a satisfactory selectivity of 20.09%, which was 8.33 times higher than that (0.49 wt%) from pure poplar. The significant increase of phenol yield might be attributed to several reasons. Firstly, during the process of NH$_4$H$_2$PO$_4$ impregnation, partial filaments in the poplar were cleaned, and the initial structure was changed to some extent owing to the acidity of NH$_4$H$_2$PO$_4$ solution. Consequently, the tight linkages between lignin and other components were weakened (Di Blasi et al., 2008), resulting in easy decomposition of biomass for phenol.

TABLE 1 | Product distributions and phenol yields under different PA-to-PL ratios at 500°C.

PA-to-PL ratio	Liquid yield (wt%)	Water content[a] (wt%)	Gas yield (wt%)	Solid yield (wt%)	Phenol yield[b] (wt%)	Phenol selectivity[c] (%)
0	50.75	34.30	17.03	32.22	0.49	1.47
0.2	36.62	54.94	14.45	48.93	3.07	13.67
0.6	34.10	60.34	11.86	54.04	4.57	20.09
1.0	31.87	64.61	9.61	58.52	3.04	14.23
1.4	28.31	68.98	8.28	63.41	2.51	12.13
1.8	26.19	76.06	6.22	67.59	1.48	7.61

[a] Based on the pyrolytic liquid product.
[b] Based on the poplar quantity in the PBs.
[c] Percentage of phenol in the organic liquid.

Besides, during the pyrolysis, $NH_4H_2PO_4$ could act as a donor of hydrogen for biomass (Zeng and Bernstein, 2019). As confirmed in previous literatures (Lu et al., 2018c; Zhang et al., 2019), the hydrogen source would exhibit positive effects on the formation of phenol by removing the substitutes on the aromatic rings. Furthermore, the co-pyrolysis of $NH_4H_2PO_4$ and poplar could generate abundant P-containing functional groups, like –O–P–C–, –C–P=O, and so on (Zhang et al., 2018b), which could improve the formation of phenol from non-lignin constituents, viz. cellulose. This point has been verified by previous study, wherein the AC activated by phosphoric acid was employed for phenol preparation from pyrolysis of cellulose (Zhang et al., 2018a). All of these factors might be responsible for the enhanced phenol yield. However, large PA-to-PL ratio could not improve but inhibit the formation of phenol, which might be ascribed to the exacerbated polycondensation and carbonization reactions to deteriorate the formation of all organic volatile compounds (Di Blasi et al., 2008).

Influence of Temperature on the Pyrolysis of Poplar Impregnated With $NH_4H_2PO_4$

The PB0.6 sample was subjected to pyrolysis under various temperatures, i.e., 450, 500, 550, 600, and 650°C. As demonstrated in **Table 2**, with the temperature rising from 450 to 650°C, the liquid yield rose gradually from 31.45 to 40.40 wt%, together with the gas yield extending from 10.65 to 17.38 wt%. While the solid yield exhibited an opposite trend and decreased from 57.90 to 42.22 wt%. Meanwhile, the water content in the liquid rose from 52.53 wt% at 450°C to 69.55 wt% at 650°C. This agreed well with biomass pyrolysis characteristics under different temperatures (Zhang et al., 2012). The high pyrolysis temperature could promote the heat transfer and cracking of macromolecular materials, thereby enhancing the generation of volatile compounds and reduction of solid product.

With the rising of pyrolytic reaction temperature, the phenol yield exhibited a tendency of first increasing and then decreasing. A passable phenol yield of 4.06 wt% was obtained at 450°C, and further increased to an expected value of 4.57 wt% at 500°C, accompanied with an obvious increase of phenol selectivity from 16.84 to 20.09%. When the temperature was further elevated, the phenol witnessed a continuous decrease. At 650°C, the phenol yield was only 2.58 wt% with a poor selectivity of 11.98%. The results manifested that the proper low temperature could promote the generation of phenol (Chang et al., 2018), while high temperature would enhance the secondary cracking and condensation reactions induced by the acidic decomposition

products of $NH_4H_2PO_4$. Consequently, the formation of phenol was inhibited and other competitive reactions were promoted (Zhang et al., 2019).

Physicochemical Properties of NPAC

The microstructure properties of NPAC were executed, with the relevant results illustrated in **Figure 2A**. According to the prominent increase of N_2 uptake capacity at low P/P_0 values (<0.2), the N_2 sorption isotherm plots of NPAC in **Figure 2A** could be classified to type I based on the IUPAC nomenclature (Thommes et al., 2015). Meanwhile, there were no obvious hysteresis loops, indicating the NPAC contained abundant micropores and a few mesopores. This could be confirmed by the pore size distribution, showing most pore sizes lower than 4 nm. In regard to the structure parameters, the SSA and total pore volume (V_{total}) of PC were only 2.0 m^2 g^{-1} and 0.008 cm^3 g^{-1}, respectively. Whereas, for the NPAC as shown in **Table 3**, its SSA (529.4 m^2 g^{-1}) and the V_{total} (0.258 cm^3 g^{-1}) were improved apparently, of which the micropores contributed 91.88 and 85.66%, respectively. $NH_4H_2PO_4$ was a common activator for preparing activated carbon (Cheng et al., 2019). In this study, the pyrolysis of poplar impregnated with $NH_4H_2PO_4$ and subsequently high temperature activation was similar to the $NH_4H_2PO_4$ activation of poplar, resulting in the enlarged SSA and V_{total}. Meanwhile, as an N and P source, the $NH_4H_2PO_4$ could improve the N and P contents in the NPAC, about 3.75 and 3.65 wt%, respectively (Xu et al., 2017).

Figure 2B illustrates the XRD patterns of PC and NPAC. Both samples had similar patterns, there were no obvious crystal diffraction peaks but two broad peaks, a prominent one at 2θ of 23.7° and a weak one at ~43.2°. The broad peak at 23.7° was ascribed to the diffraction plane of (002), representing the graphitic stacking (Zou and Jiang, 2020). While the weak peak was ascribed to the diffraction plane of (100), indicating a limited degree of graphitization (Raj et al., 2018). The two peaks indicated that both PC and NPAC were with highly amorphous states (Wang et al., 2019).

The XPS spectra of N *1s* and P *2p* of NPAC are depicted in the **Figure 3**. Four peaks centered at 398.30, 399.65, 401.20, and 402.39 eV were observed in the N *1s* spectrum, which represented pyridinic-N (N-6), pyrrolic-N (N-5), quaternary-N (N-Q), and oxidized N (N-X), respectively (Chen et al., 2016). As indicated above, the N in NPAC originated from the reaction of NH_3 with O-containing groups during the pyrolysis

TABLE 2 | Product distributions and phenol yields at different temperatures with PA-to-PL ratio of 0.6.

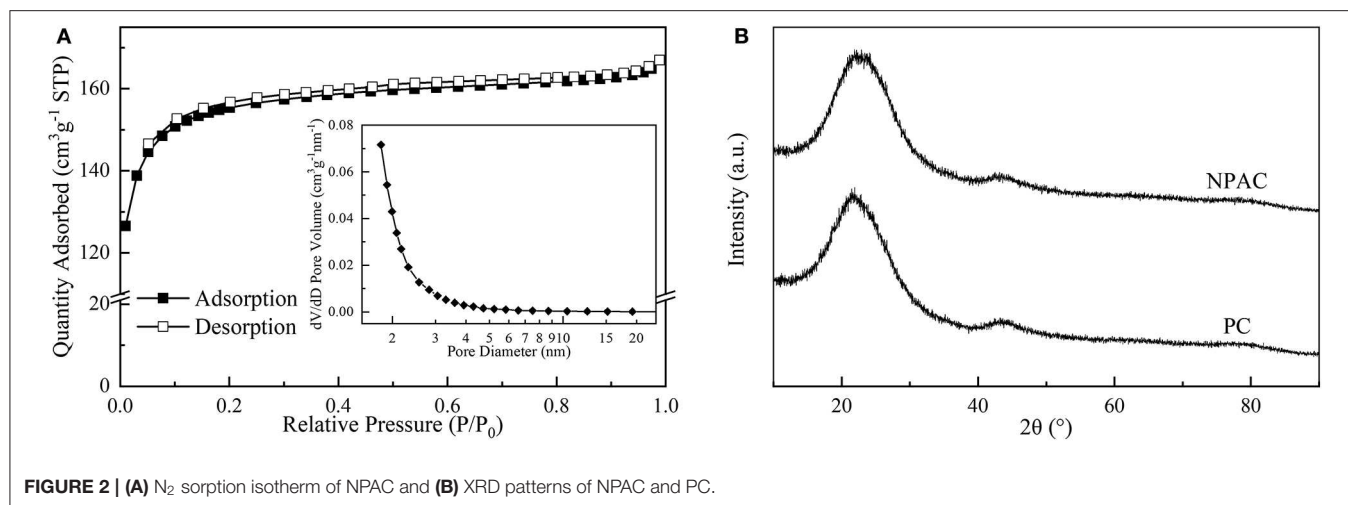| Temperature (°C)	Liquid yield (wt%)	Water content (wt%)	Gas yield (wt%)	Solid yield (wt%)	Phenol yield (wt%)	Phenol selectivity (%)
450	31.45	52.53	10.65	57.90	4.06	16.84
500	34.10	60.34	11.86	54.04	4.57	20.09
550	36.41	65.27	14.24	49.35	3.47	16.43
600	38.31	68.75	15.75	45.94	2.83	14.72
650	40.40	69.55	17.38	42.22	2.58	11.98

FIGURE 2 | **(A)** N$_2$ sorption isotherm of NPAC and **(B)** XRD patterns of NPAC and PC.

TABLE 3 | Microstructure properties and elemental composition of NPAC.

SSA (m^2 g^{-1})		Pore volume (cm^3 g^{-1})		Diameter (nm)	Elemental composition (wt%)				
S$_{BET}$	S$_{mic}^a$	V$_{total}^b$	V$_{mic}^c$	D$_{average}$	C	H	O	N	P
529.4	486.4	0.258	0.221	1.95	66.56	1.12	19.33	3.75	3.65

^{a,c}t-Plot micropore area and micropore volume.
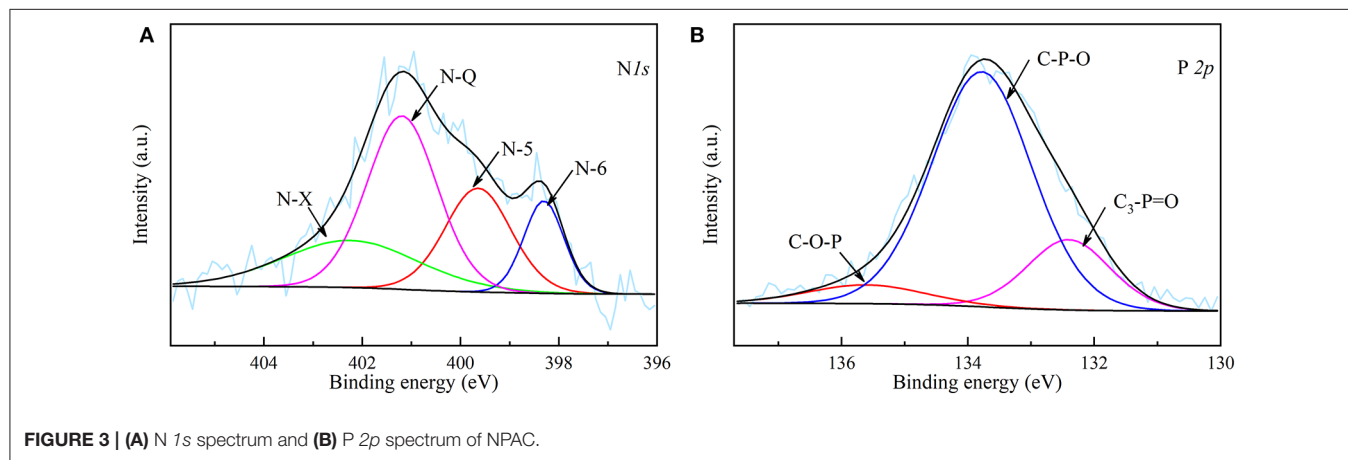^{b}P/P$_0$ = 0.989.

FIGURE 3 | **(A)** N $1s$ spectrum and **(B)** P $2p$ spectrum of NPAC.

process. The N-5 and N-6 were believed to be the cyclization products of N-containing intermediates, while the N-Q might come from the condensation reactions of N-6 (Chen et al., 2018a). These N species possessed different contributions to the electrochemical properties. In General, the N-5 and N-6 can improve the pseudocapacitance, while the N-Q can enhance the conductivity (Fu et al., 2019; Ma et al., 2020). For the P species in **Figure 3B**, the band at 132.4 eV was attributed to C$_3$-P=O, the peaks centered at 133.78 and 135.61 eV were considered to be C–O–P and C–P–O (Liu et al., 2015). The introduction of P could not only improve the pseudocapacitance, but also widen the operating voltage window of the capacitor (Ma et al., 2018).

Electrochemical Performance of NPAC

The electrochemical performances of NPAC were systemically characterized via CV, GCD, and EIS. **Figure 4A** illustrates the CV curves of PC and NPAC at 5 mV s^{-1}. Compared with PC, NPAC possessed better rectangularity and larger surface area, resulting from its high SSA and the N and P co-doping in carbon (Wu et al., 2015). With the rise of voltage scan rates, the corresponding CV curves of NPAC still displayed similar rectangular shapes with certain deformation, as illustrated in **Figure 4B**. Besides, there were no obvious peaks, revealing the perfect electrochemical performance of NPAC with lower inner resistance (Li et al., 2019).

Figure 5A illustrates the GCD curves of NPAC obtained under various current densities (1–20 A g^{-1}). Apparently, all the
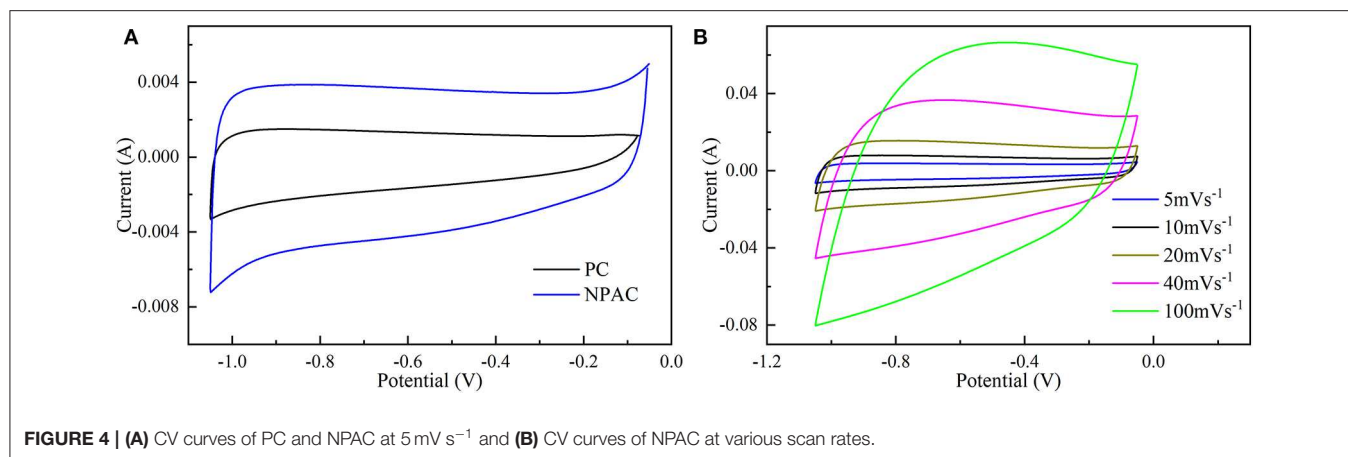
FIGURE 4 | (A) CV curves of PC and NPAC at 5 mV s^{-1} and (B) CV curves of NPAC at various scan rates.
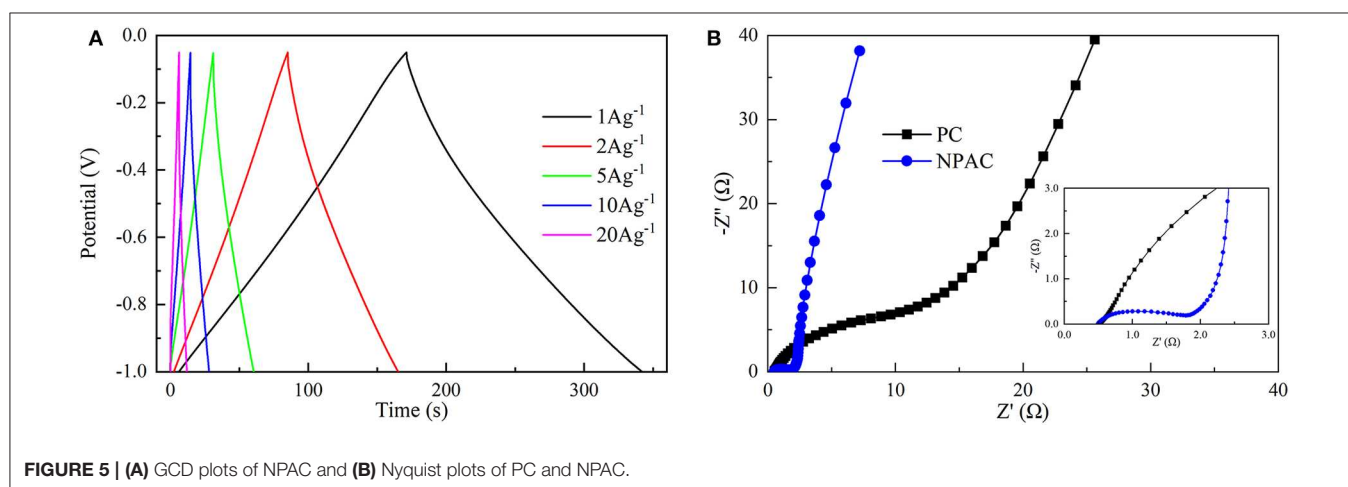

FIGURE 5 | (A) GCD plots of NPAC and (B) Nyquist plots of PC and NPAC.

GCD curves exhibited high triangularity. The linear relationship between voltage and time represented excellent electrochemical capacitance behavior (Chen et al., 2018b). Further, the C_g values were calculated and inversely correlated with current densities. The maximum C_g of 181.3 F g^{-1} was obtained at 1 A g^{-1}. The higher current densities (20 A g^{-1}) led to an attenuation of 30% in C_g. In other words, the capacitance retention remained about 70%, higher than many relevant values in previous researches (Wang et al., 2013a; Xu et al., 2019). This indicated the excellent electrochemical capacitive properties. Generally, under high charging/discharging current densities, the charging could finish quickly in high speed. However, the large impedance caused by the micropores in NPAC would lead to the charging time constant too long to charge completely, resulting in the decrease of C_gs under high current densities (Divya and Rajalakshmi, 2020).

Figure 5B illustrates the Nyquist plots of PC and NPAC. Compared with PC, the NPAC possessed a semicircle with small diameter at high frequency. The diameter reflected the charge transfer resistance (R_{ct}) (Wei et al., 2015), while the intersection point of the abscissa axis and semicircle represented the equivalent series resistance (ESR) (Sun et al., 2019). Apparently, the R_{ct} of NPAC was nearly 1.2 Ω, much lower than that of PC

(about 22 Ω). The ESR of NPAC was about 0.5 Ω, indicating the good conductivity of NPAC (Chen et al., 2016; Zhang et al., 2017). The larger line slope of NPAC close to vertical at the low-frequency region indicated its excellent electrical capacitance characteristics (Yang et al., 2018). In brief, the high content of heteroatoms (N and P) and good porous structure enabled the NPAC with the promising potential as a supercapacitor.

CONCLUSIONS

Pyrolysis of $NH_4H_2PO_4$-impregnated biomass provided a promising way for polygeneration of phenol and NPAC. A lab-scale device was utilized for the experiments to reveal the effects of PA-to-PL ratio as well as pyrolytic temperature on the products formation and phenol yield. The pyrolytic solid product obtained under the maximal phenol yield condition was used to prepare NPAC by direct high temperature activation. The results indicated that the highest phenol yield attained 4.57 wt% with a satisfactory selectivity of 20.09% at 500°C and PA-to-PL ratio of 0.6. The as-obtained NPAC exhibited promising electrochemical performance, with an excellent C_g of 181.3 F g^{-1} at 1 A g^{-1}, and thus, could be used as a supercapacitor electrode material.

DATA AVAILABILITY STATEMENT

The raw data supporting the conclusions of this article will be made available by the authors, without undue reservation, to any qualified researcher.

AUTHOR CONTRIBUTIONS

KL: conceptualization, methodology, and writing-original draft. BW: investigation, and writing-review and editing. DB: methodology. DN: investigation and validation. QL: conceptualization, supervision, writing-review and editing, and funding acquisition.

ACKNOWLEDGMENTS

SUPPLEMENTARY MATERIAL

The Supplementary Material for this article can be found online at: https://www.frontiersin.org/articles/10.3389/fchem. 2020.00436/full#supplementary-material

REFERENCES

Brueckner, T. M., Pickup, P. G., and Hawboldt, K. (2020). Improvement of bark pyrolysis oil and value added chemical recovery by pervaporation. *Fuel. Process. Technol.* 199:106292. doi: 10.1016/j.fuproc.2019.106292

Bu, Q., Lei, H., Ren, S., Wang, L., Zhang, Q., Tang, J., et al. (2012). Production of phenols and biofuels by catalytic microwave pyrolysis of lignocellulosic biomass. *Bioresour. Technol.* 108, 274–279. doi: 10.1016/j.biortech.2011.12.125

Chang, G., Miao, P., Yan, X., Wang, G., and Guo, Q. (2018). Phenol preparation from catalytic pyrolysis of palm kernel shell at low temperatures. *Bioresour. Technol.* 253, 214–219. doi: 10.1016/j.biortech.2017.12.084

Chen, D., Zhou, J., Zhang, Q., and Zhu, X. (2014). Evaluation methods and research progresses in bio-oil storage stability. *Renew. Sust. Energ. Rev.* 40, 69–79. doi: 10.1016/j.rser.2014.07.159

Chen, H., Wei, H., Fu, N., Qian, W., Liu, Y., Lin, H., et al. (2018b). Nitrogen-doped porous carbon using ZnCl₂ as activating agent for high-performance supercapacitor electrode materials. *J. Mater. Chem.* 53, 2669–2684. doi: 10.1007/s10853-017-1453-3

Chen, W., Li, K., Xia, M., Chen, Y., Yang, H., Chen, Z., et al. (2018a). Influence of NH₃ concentration on biomass nitrogen-enriched pyrolysis. *Bioresour. Technol.* 263, 350–357. doi: 10.1016/j.biortech.2018.05.025

Chen, W., Yang, H., Chen, Y., Chen, X., Fang, Y., and Chen, H. (2016). Biomass pyrolysis for nitrogen-containing liquid chemicals and nitrogen-doped carbon materials. *J. Anal. Appl. Pyrol.* 120, 186–193. doi: 10.1016/j.jaap.2016.05.004

Chen, X., Che, Q., Li, S., Liu, Z., Yang, H., Chen, Y., et al. (2019). Recent developments in lignocellulosic biomass catalytic fast pyrolysis: Strategies for the optimization of bio-oil quality and yield. *Fuel. Process. Technol.* 196:106180. doi: 10.1016/j.fuproc.2019.106180

Cheng, B, Zeng, F., Chen, W, Cheng, H., Zeng, R., and Jiang, H. (2019). Nontemplating porous carbon material from polyphosphamide resin for supercapacitors. *iScience* 12, 204–215. doi: 10.1016/j.isci.2019.01.016

Di Blasi, C., Branca, C., and Galgano, A. (2007). Effects of diammonium phosphate on the yields and composition of products from wood pyrolysis. *Ind. Eng. Chem. Res.* 46, 430–438. doi: 10.1021/ie0612616

Di Blasi, C., Branca, C., and Galgano, A. (2008). Thermal and catalytic decomposition of wood impregnated with sulfur-and phosphorus-containing ammonium salts. *Polym. Degrad. Stabil.* 93, 335–346. doi: 10.1016/j.polymdegradstab.2007.12.003

Divya, P., and Rajalakshmi, R. (2020). Renewable low cost green functional mesoporous electrodes from *Solanum lycopersicum* leaves for supercapacitors. *J. Energy Storage* 27:101149. doi: 10.1016/j.est.2019.101149

Dong, C., Zhang, Z., Lu, Q., and Yang, Y. (2012). Characteristics and mechanism study of analytical fast pyrolysis of poplar wood. *Energ. Convers. Manage.* 57, 49–59. doi: 10.1016/j.enconman.2011.12.012

Duan, D., Lei, H., Wang, Y., Ruan, R., Liu, Y., Ding, L., et al. (2019). Renewable phenol production from lignin with acid pretreatment and *ex-situ* catalytic pyrolysis. *J. Clean. Prod.* 231, 331–340. doi: 10.1016/j.jclepro.2019.05.206

Fu, D., Chen, Z., Yu, C., Song, X., and Zhong, W. (2019). Bimetallic-organic coordination polymers to prepare N-doped hierarchical porous carbon for high performance supercapacitors. *Prog. Nat. Sci. Mater.* 29, 495–503. doi: 10.1016/j.pnsc.2019.08.014

Kan, T., Strezov, V., and Evans, T. J. (2016). Lignocellulosic biomass pyrolysis: a review of product properties and effects of pyrolysis parameters. *Renew. Sust. Enegr. Rev.* 57, 1126–1140. doi: 10.1016/j.rser.2015.12.185

Kim, J. K., Yoo, Y., and Kang, Y. C. (2020). Scalable green synthesis of hierarchically porous carbon microspheres by spray pyrolysis for high-performance supercapacitors. *Chem Eng. J.* 382:122805. doi: 10.1016/j.cej.2019.122805

Lazaridis, P. A., Fotopoulos, A. P., Karakoulia, S. A., and Triantafyllidis, K. S. (2018). Catalytic fast pyrolysis of kraft lignin with conventional, mesoporous and nanosized ZSM-5 zeolite for the production of alkyl-phenols and aromatics. *Front. Chem.* 6:295. doi: 10.3389/fchem.2018.00295

Li, K., Chen, W., Yang, H., Chen, Y., Xia, S., Xia, M., et al. (2019). Mechanism of biomass activation and ammonia modification for nitrogen-doped porous carbon materials. *Bioresour. Technol.* 280, 260–268. doi: 10.1016/j.biortech.2019.02.039

Li, K., Wang, Z., Zhang, G., Cui, M., Lu, Q., Yang, Y (2020). Selective production of monocyclic aromatic hydrocarbons from *ex situ* catalytic fast pyrolysis of pine over the HZSM-5 catalyst with calcium formate as a hydrogen source. *Sustain. Energ. Fuels* 4, 538–548. doi: 10.1039/C9SE00605B

Li, K., Zhang, L., Zhu, L., and Zhu, X. (2017). Comparative study on pyrolysis of lignocellulosic and algal biomass using pyrolysis-gas chromatography/mass spectrometry. *Bioresour. Technol.* 234, 48–52. doi: 10.1016/j.biortech.2017.03.014

Li, K., Zhu, C., Zhang, L., and Zhu, X. (2016). Study on pyrolysis characteristics of lignocellulosic biomass impregnated with ammonia source. *Bioresour. Technol.* 209, 142–147. doi: 10.1016/j.biortech.2016.02.136

Liang, C., Gascó, G., Fu, S., Méndez, A., and Paz-Ferreiro, J. (2016). Biochar from pruning residues as a soil amendment: effects of pyrolysis temperature and particle size. *Soil. Till. Res.* 164, 3–10. doi: 10.1016/j.still.2015.10.002

Liu, C., Zhang, Y., and Huang, X. (2014). Study of guaiacol pyrolysis mechanism based on density function theory. *Fuel. Process. Technol.* 123, 159–165. doi: 10.1016/j.fuproc.2014.01.002

Liu, J., Wang, Z., Wu, X., Yuan, X., Hu, J., Zhou, Q., et al. (2015). Porous carbon derived from disposable shaddock peel as an excellent catalyst toward VO^{2+}/VO_2^+ couple for vanadium redox battery. *J. Power Sources* 299, 301–308. doi: 10.1016/j.jpowsour.2015.09.004

Lu, C., Huang, Y., Wu, Y., Li, J., and Cheng, J. (2018a). Camellia pollen-derived carbon for supercapacitor electrode material. *J. Power Sources* 394, 9–16. doi: 10.1016/j.jpowsour.2018.05.032

Lu, Q., Zhang, Z., Wang, X., Guo, H., Cui, M., and Yang, Y. (2018c). Catalytic fast pyrolysis of biomass impregnated with potassium phosphate in a hydrogen atmosphere for the production of phenol and activated carbon. *Front. Chem.* 6:32. doi: 10.3389/fchem.2018.00032

Lu, Q., Zhang, Z., Yang, X., Dong, C., and Zhu, X. (2013). Catalytic fast pyrolysis of biomass impregnated with K₃PO₄ to produce phenolic compounds: analytical Py-GC/MS study. *J. Anal. Appl. Pyrol.* 104, 139–145. doi: 10.1016/j.jaap.2013.08.011

Lu, Q., Zhou, M., Li, W., Wang, X., Cui, M., and Yang, Y. (2018b). Catalytic fast pyrolysis of biomass with noble metal-like catalysts to produce high-grade bio-oil: analytical Py-GC/MS study. *Catal. Today*, 302, 169–179. doi: 10.1016/j.cattod.2017.08.029

Ma, W., Xie, L., Dai, L., Sun, G., Chen, J., Su, F., et al. (2018). Influence of phosphorus doping on surface chemistry and capacitive behaviors of porous carbon electrode. *Electrochim. Acta* 266, 420–430. doi: 10.1016/j.electacta.2018.02.031

Ma, Y., Wu, D., Wang, T., and Jia, D. (2020). Nitrogen, phosphorus co-doped carbon obtained from amino acid based resin xerogel as efficient electrode for supercapacitor. *ACS. Appl. Energ. Mat.* 3, 957–969. doi: 10.1021/acsaem.9b02032

Muneer, B., Zeeshan, M., Qaisar, S., Razzaq, M., and Iftikhar, H. (2019). Influence of *in-situ* and *ex-situ* HZSM-5 catalyst on co-pyrolysis of corn stalk and polystyrene with a focus on liquid yield and quality. *J. Clean. Prod.* 237:117762. doi: 10.1016/j.jclepro.2019.117762

Raj, C. J., Rajesh, M., Manikandan, R., Yu, K. H., Anusha, J., Ahn, J. H., et al. (2018). High electrochemical capacitor performance of oxygen and nitrogen enriched activated carbon derived from the pyrolysis and activation of squid gladius chitin. *J. Power Sources* 386, 66–76. doi: 10.1016/j.jpowsour.2018.03.038

Su, Y., Zhang, Y., Qi, J., Xue, T., Xu, M., Yang, J., et al. (2020). Upgrading of furans from *in situ* catalytic fast pyrolysis of xylan by reduced graphene oxide supported Pt nanoparticles. *Renew. Energy* 152, 94–101. doi: 10.1016/j.renene.2020.01.036

Sun, Q., Li, Y., and He, T. (2019). The excellent capacitive capability for N, P-doped carbon microsphere/reduced graphene oxide nanocomposites in H_2SO_4/KI redox electrolyte. *J. Mater. Sci.* 54, 7665–7678. doi: 10.1007/s10853-019-03414-x

Thommes, M., Kaneko, K., Neimark, A. V., Olivier, J. P., Rodriguez-Reinoso, F., Rouquerol, J., et al. (2015). Physisorption of gases, with special reference to the evaluation of surface area and pore size distribution (IUPAC Technical Report). *Pure. Appl. Chem.* 87, 1051–1069. doi: 10.1515/pac-2014-1117

Wang, C., Sun, L., Zhou, Y., Wan, P., Zhang, X., and Qiu, J. (2013a). P/N co-doped microporous carbons from H_3PO_4-doped polyaniline by *in situ* activation for supercapacitors. *Carbon* 59, 537–546. doi: 10.1016/j.carbon.2013.03.052

Wang, C., Zhou, Y., Sun, L., Wan, P., Zhang, X., and Qiu, J. (2013b). Sustainable synthesis of phosphorus-and nitrogen-co-doped porous carbons with tunable surface properties for supercapacitors. *J. Power Sources* 239, 81–88. doi: 10.1016/j.jpowsour.2013.03. 126

Wang, J., Li, Y., Yan, L., and Qu, Y. (2018b). Nitrogen-phosphorus co-doped porous carbon based on peanut shell for surpercapactior. *Int. J. Electrochem. Sci.* 13, 6259–6271. doi: 10.20964/2018.07.47

Wang, J., and Wang, S. (2019). Preparation, modification and environmental application of biochar: a review. *J. Clean. Prod.* 227, 1002–1022. doi: 10.1016/j.jclepro.2019.04.282

Wang, L., Zhang, R., Li, J., Guo, L., Yang, H., Ma, F., et al. (2018a). Comparative study of the fast pyrolysis behavior of ginkgo, poplar, and wheat straw lignin at different temperatures. *Ind. Crop. Prod.* 122, 465–472. doi: 10.1016/j.indcrop.2018.06.038

Wang, X., Liu, Y., Chen, M., Luo, M., Yang, P., Chen, W., et al. (2019). Direct microwave conversion from lignin to micro/meso/macroporous carbon for high-performance symmetric supercapacitors. *ChemElectroChem* 6, 4789–4800. doi: 10.1002/celc.201901315

Wei, T., Wei, X., Gao, Y., and Li, H. (2015). Large scale production of biomass-derived nitrogen-doped porous carbon materials for supercapacitors. *Electrochim. Acta* 169, 186–194. doi: 10.1016/j.electacta.2015.04.082

Wu, J., Jin, C., Yang, Z., Tian, J., and Yang, R. (2015). Synthesis of phosphorus-doped carbon hollow spheres as efficient metal-free electrocatalysts for oxygen reduction. *Carbon* 82, 562–571. doi: 10.1016/j.carbon.2014.11.008

Xu, D., Su, Y., Zhang, S., and Xiong, Y. (2019). Highly porous N-doped carbons production from biomass for high-performance supercapacitors without

chemical nitrogen-containing dopants. *Energy. Sources A* 42, 1797–1807. doi: 10.1080/15567036.2019.1604890

Xu, D., Tong, Y., Yan, T., Shi, L., and Zhang, D. (2017). N, P-codoped meso-/microporous carbon derived from biomass materials via a dual-activation strategy as high-performance electrodes for deionization capacitors. *ACS Sustain. Chem. Eng.* 5, 5810–5819. doi: 10.1021/acssuschemeng.7b00551

Xu, D. L., Gao, Y. X., Lin, Z. X., Gao, W. R., Zhang, H., Karnowo, K., et al. (2020). Application of biochar derived from pyrolysis of waste fiberboard on tetracycline adsorption in aqueous solution. *Front. Chem.* 7:11. doi: 10.3389/fchem.2019.00943

Yaman, E., Yargic, A. S., Ozbay, N., Uzun, B. B., Kalogiannis, K. G., Stefanidis, S. D., et al. (2018). Catalytic upgrading of pyrolysis vapours: effect of catalyst support and metal type on phenolic content of bio-oil. *J. Clean. Prod.* 185, 52–61. doi: 10.1016/j.jclepro.2018.03.033

Yang, J., Wang, Y., Luo, J., and Chen, L. (2018). Highly nitrogen-doped graphitic carbon fibers from sustainable plant protein for supercapacitor. *Ind. Crop. Prod.* 121, 226–235. doi: 10.1016/j.indcrop.2018.05.013

Ye, X., Lu, Q., Wang, X., Guo, H., Cui, M., Dong, C., et al. (2017). Catalytic fast pyrolysis of cellulose and biomass to selectively produce levoglucosenone using activated carbon catalyst. *ACS Sustain. Chem. Eng.* 5, 10815–10825. doi: 10.1021/acssuschemeng.7b02762

Zeng, Z., and Bernstein, E. R. (2019). Ammonium perchlorate and ammonium dihydrogen phosphate as energetic materials: comparison to ammonium nitrate. *J. Phys. Chem. C* 123, 12149–12153. doi: 10.1021/acs.jpcc.9b02410

Zhang, M., Resende, F. L., Moutsoglou, A., and Raynie, D. E. (2012). Pyrolysis of lignin extracted from prairie cordgrass, aspen, and Kraft lignin by Py-GC/MS and TGA/FTIR. *J. Anal. Appl. Pyrol.* 98, 65–71. doi: 10.1016/j.jaap.2012.05.009

Zhang, S., Tian, K., Cheng, B., and Jiang, H. (2017). Preparation of N-doped supercapacitor materials by integrated salt templating and silicon hard templating by pyrolysis of biomass wastes. *ACS Sustain. Chem. Eng.* 5, 6682–6691. doi: 10.1021/acssuschemeng.7b00920

Zhang, Y., Lei, H., Yang, Z., Duan, D., Villota, E., and Ruan, R. (2018b). From glucose-based carbohydrates to phenol-rich bio-oils integrated with syngas production via catalytic pyrolysis over an activated carbon catalyst. *Green. Chem.* 20, 3346–3358. doi: 10.1039/C8GC00593A

Zhang, Y., Lei, H., Yang, Z., Qian, K., and Villota, E. (2018a). Renewable high-purity mono-phenol production from catalytic microwave-induced pyrolysis of cellulose over biomass-derived activated carbon catalyst. *ACS Sustain. Chem. Eng.* 6, 5349–5357. doi: 10.1021/acssuschemeng.8b00129

Zhang, Z., Li, K., Ma, S., Cui, M., Lu, Q., and Yang, Y. (2019). Fast pyrolysis of biomass catalyzed by magnetic solid base catalyst in a hydrogen atmosphere for selective production of phenol. *Ind. Crop. Prod.* 137, 495–500. doi: 10.1016/j.indcrop.2019.05.066

Zhao, X., Wang, S., and Wu, Q. (2017). Nitrogen and phosphorus dual-doped hierarchical porous carbon with excellent supercapacitance performance. *Electrochim. Acta* 247, 1140–1146. doi: 10.1016/j.electacta.2017.07.077

Zou, Z., and Jiang, C. (2020). Hierarchical porous carbons derived from leftover rice for high performance supercapacitors. *J. Alloy Compd.* 815:152280. doi: 10.1016/j.jallcom.2019.152280